

Structural properties of PZT/BFO multilayer thin films

Seo-Hyeon Jo^a, Dae-Young Kim^a, Gwang-Ho Jeong^a, Sung-Gap Lee^{a,*} and Young-Gon Kim^b

^aDept. of Ceramic Engineering, Eng. Res. Insti., Gyeongsang National University, Jinju-Si, Korea

^bDept. of Photoelectronics Information, Chosun University College of Science & Technology, Gwangju, Korea

PZT/BFO multilayer thin films were fabricated by the spin-coating method on Pt(200 nm)/Ti(10 nm)/SiO₂(100 nm)/p-Si(100) substrates using BiFeO₃ and Pb(Zr_{0.52}Ti_{0.48})O₃ metal alkoxide solutions. All PZT/BFO multilayer thin films show the typical XRD pattern of a polycrystalline rhombohedral structure and a uniform and void free grain microstructure. The thickness of the BFO and PZT film by one-cycle of drying/sintering was approximately 40 nm and all films consist of fine grains with a relatively flat surface morphology. PZT/Pt and Pt/Ti interfaces became more and more rough interfacial layers with an increase in the number of coatings because the diffusion of Pb from PZT film into the Pt bottom electrode and the diffusion of Ti was more advanced with an increase in the number of annealing process. All the films showed hysteresis loops with high rectangularity. The remanent polarizations of PZT/BFO and PZT/BFO/PZT multilayer thin films are 47.85 C/cm² and 39.97 C/cm², respectively.

Key words: BFO, PZT, Multilayer film, Sol-gel method, Hysteresis loop.

Introduction

Recently increasing attention has been focused on multiferroic thin films, which exhibit simultaneously ferroelectric, ferromagnetic, antiferromagnetic and ferroelastic behavior. However, most of the multiferroic materials are not promising for device applications because their transition temperatures for ferroelectricity or magnetic ordering are lower than room temperature. On the other hand, BiFeO₃(BFO), with a space group R3c, has higher transition temperature, that is, a Curie temperature of 850 °C and a Neel temperature of 370 °C [1]. However, BFO has serious problems as a ferroelectric material that is, quite a large leakage current density, especially at room temperature. So, dielectric breakdown occurs easily even at a low field, thereby indicating the difficult in poling a film. To overcome this problem, various approaches have been proposed, including the substitution techniques using Mn, Ti at B-sites and/or La and Nd at A-sites [2-4] and the formation of a solid solution with Pb(Zr,Ti)O₃ and BaTiO₃ compositions [5, 6].

There are many reports on the reduction in the leakage current induced by doping and the formation of the solid solution. In these investigations, the capacitor structure formed from metal-insulator-metal is used for the current measurement. It should be noted that the current measured in the capacitor structure includes contributions of the grain boundaries or the microstructure of the films. We have already reported on the good dielectric properties,

especially high remanent polarization and low leakage current densities of PZT heterolayered thin films which they were alternately spin-coated using tetragonal PZT(20/80) and rhombohedral PZT(80/20) metal alkoxide solutions [7]. In this study, BFO/PZT multilayer thin films were prepared by a sol-gel method, which were spin-coated on platinized Si substrates alternately using the BFO and PZT metal alkoxide solutions. The objective of the present study is to investigate the space charge distribution behavior of PZT/BFO multilayer thin films to reduce the leakage current.

Experiments

BiFeO₃ and Pb(Zr_{0.52}Ti_{0.48})O₃ with excess Pb-acetate 10 mol% precursor solutions were prepared by a sol-gel method from Bi-nitrate pentahydrate [Bi(NO₃)₃·5H₂O], Fe-nitrate nonahydrate [Fe(NO₃)₃·9H₂O], Pb-acetate trihydrate [Pb(CH₃CO₂)₂·3H₂O], Zr n-propoxide [Zr(OCH₂CH₂CH₃)₄] and Ti iso-propoxide {Ti[OCH(CH₃)₂]₄} as starting materials, and 2-methoxyethanol as the solvent. The PZT precursor solution was passed through a syringe filter and spin-coated on Pt(200 nm)/Ti(10 nm)/SiO₂(100 nm)/p-Si(100) substrates using a spinner operated at 4000 rpm for 30 s to form the first layer. These PZT films were dried at 300 °C for 30 minutes to remove the organic materials, and sintered at 600 °C for 30 minutes to crystallize them into the perovskite structure. Also the BFO precursor solution was then spin-coated and dried on the PZT films under the same conditions, and sintered at 600 °C for 10 minutes to form the second BFO layer. This procedure was repeated several times, and BFO/PZT multilayer thin films were fabricated.

The crystallinity of BFO/PZT multilayer films were

*Corresponding author:
Tel : +82-55-772-1687
Fax: +82-55-772-1689
E-mail: lsgap@gnu.ac.kr

analyzed by X-ray diffraction (XRD) and surface and cross-sectional morphologies of the films were examined by scanning electron microscopy (SEM). For ferroelectric properties measurements, Pt films were DC sputter-deposited on the BFO/PZT films as the top electrode with a diameter of 250 nm.

Results and Discussion

Fig. 1(a) and 1(b) show the X-ray diffraction patterns of BFO thin films coated on a Pt electrode and PZT thin film, respectively. The (111) diffraction peaks of BFO and PZT cannot be observed because they overlap with the Pt (111) peak. Fig. 1(a) shows the typical XRD pattern of a rhombohedral structure, and a second phase such as $\text{Bi}_2\text{Fe}_4\text{O}_9$ or a preferred orientation were not observed. However, the XRD pattern of the BFO thin film coated on a PZT layer depicted in Fig. 1(b) shows that the peak splits of (101)/(110) at a 2-theta value of 32° occurred and were shifted to a lower angle side. This property may be understood in terms of the effect of the difference of the lower layer. And it can be assumed that the lower PZT layers play an important role of nucleation sites or a seeding layer for the formation of the upper BFO layers. Fig. 1(c) shows the X-ray diffraction pattern of a PZT/BFO/PZT multilayer thin film. A polycrystalline perovskite phase with the rhombohedral structure of PZT is observed clearly. On the other hand, a weak (110) of the lower BFO layer appears in the PZT film deposited on the Pt/PZT/BFO layer. The peak splits of (100)/(001) and (101)/(110) at 2-theta values of 21° and 31° occurred, respectively, and were shifted to the lower angle side compared with a pure PZT(52/48) thin film [8]. As mentioned earlier, the crystal growth of the upper PZT layer can be influenced by the lower BFO layers and the crystallization behavior of the resultant film has been controlled by choosing the initial layer or seeding layer.

Fig. 2(a)-(c) show the surface FE-SEM micrographs of BFO, PZT/BFO and PZT/BFO/PZT multilayer thin films, respectively. The BFO thin film (Fig. 2(a)) showed a uniform and void free grain structure with an average grain size of 120–130 nm. The PZT/BFO multilayer thin

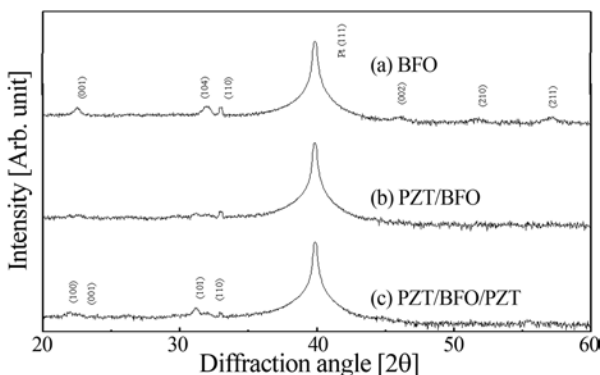


Fig. 1. X-ray diffraction patterns for (a) BFO film, (b) PZT/BFO film and (c) PZT/BFO/PZT film.

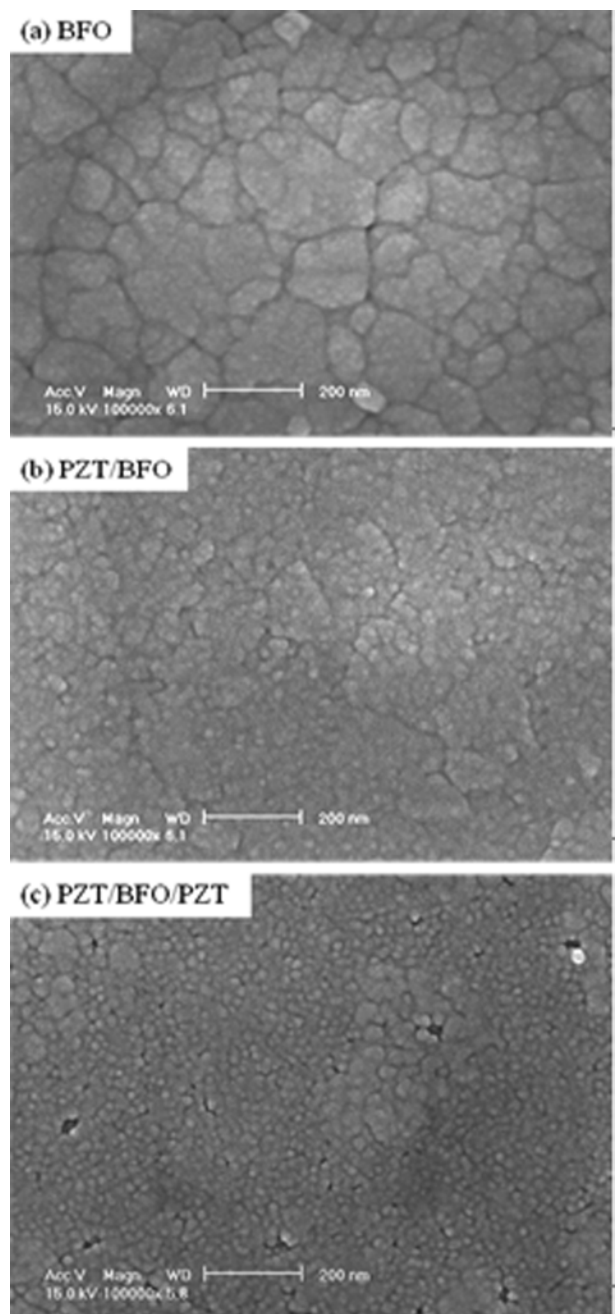


Fig. 2. FE-SEM images of surface micrographs for (a) BFO film, (b) PZT/BFO film and (c) PZT/BFO/PZT film.

film (Fig. 2(b)) showed a uniform and void free grain structure, however the grain size is smaller than that of BFO film. In the PZT/BFO/PZT multilayer thin film (Fig. 2(c)), small grains are observed and large clusters partially agglomerated from these grains. The grain size of the PZT/BFO/PZT thin films are considered to be smaller than those of the BFO thin films. According to a report by Matsuno and Sasaki [9], the PZT bulk is produced in two steps. The first step is a reaction of PbO , TiO_2 to PbTiO_3 . The second step is a reaction of PbTiO_3 , ZrO_2 and PbO to PZT at a higher temperature. This reaction mechanism indicates that the crystallization temperature

of PZT with a Ti-richer composition is lower. In general, the PZT films with a Zr-rich composition show a fine and void free grain structure while the PZT films with a Ti-rich composition have a large grain structure [10]. It is difficult to determine the correct reason for this with the measurements shown. We suggest that this is due to the larger amount of nucleation sites in the PZT thin films, although the grain size of the BFO film is the largest.

Fig. 3(a)-(c) show cross-sectional SEM micrographs

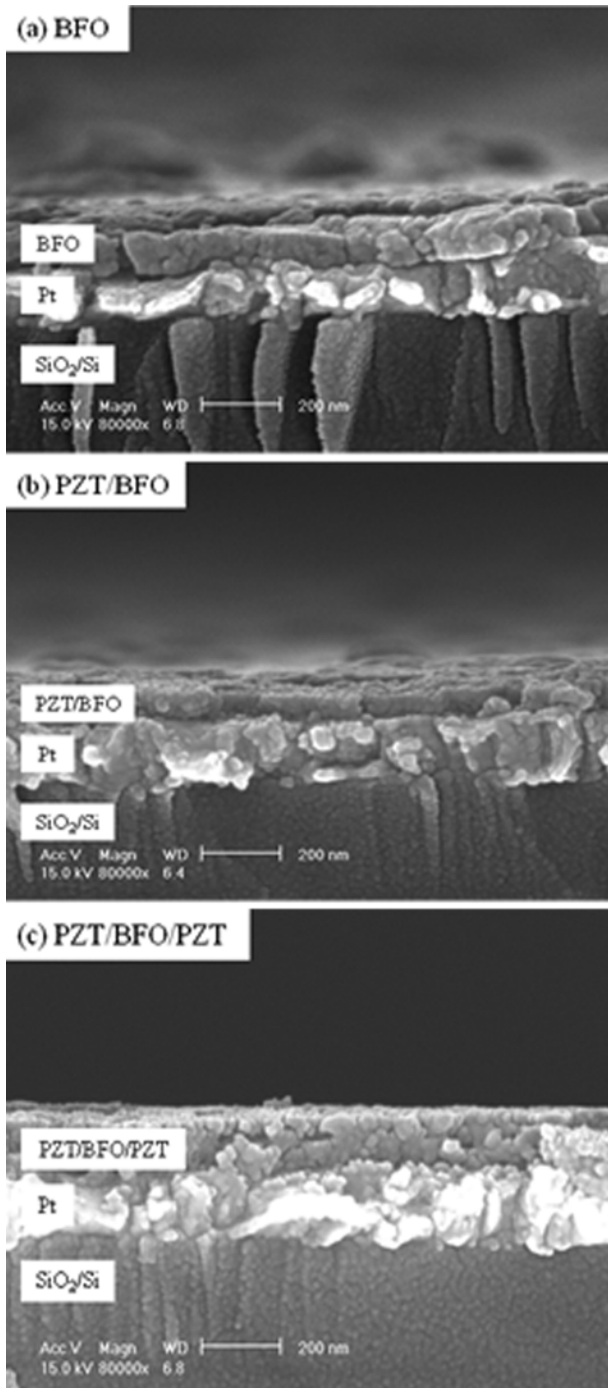


Fig. 3. FE-SEM images of cross-sectional micrographs for (a) BFO film, (b) PZT/BFO film and (c) PZT/BFO/PZT film.

of BFO, PZT/BFO and PZT/BFO/PZT multilayer thin films, respectively. The BFO thin film (Fig. 3(a)) is coated 3 times. The electrical properties of the BFO thin films coated 1 and 2 times could not be measured because the thicknesses of these films were too thin. The thickness of BFO and PZT films by one-cycle of drying/sintering was approximately 40 nm and all films consist of fine grains with a relatively flat surface morphology. As shown in Fig. 3(b) and 3(c), the PZT/Pt and Pt/Ti interfaces became more and more rough interfacial layers with an increase in the number of coatings. This phenomenon can probably be explained by the fact that the diffusion of Pb from PZT film into the Pt bottom electrode and the diffusion of Ti was more advanced with an increase in the number of coatings, in other words, an increase in the number of annealing processes.

Fig. 4(a) and 4(b) show the polarization-electric field (P-E) hysteresis loops of the PZT/BFO and PZT/BFO/PZT multilayer thin films measured at 300 K with a frequency of 100 Hz, respectively. All the films showed hysteresis loops with high rectangularity. The hysteresis loops in Fig. 4 show voltage shifts toward a negative bias field. It is suggested that the internal bias field at the interface between the lower electrode and PZT films was induced by the difference of thermal history of the upper and

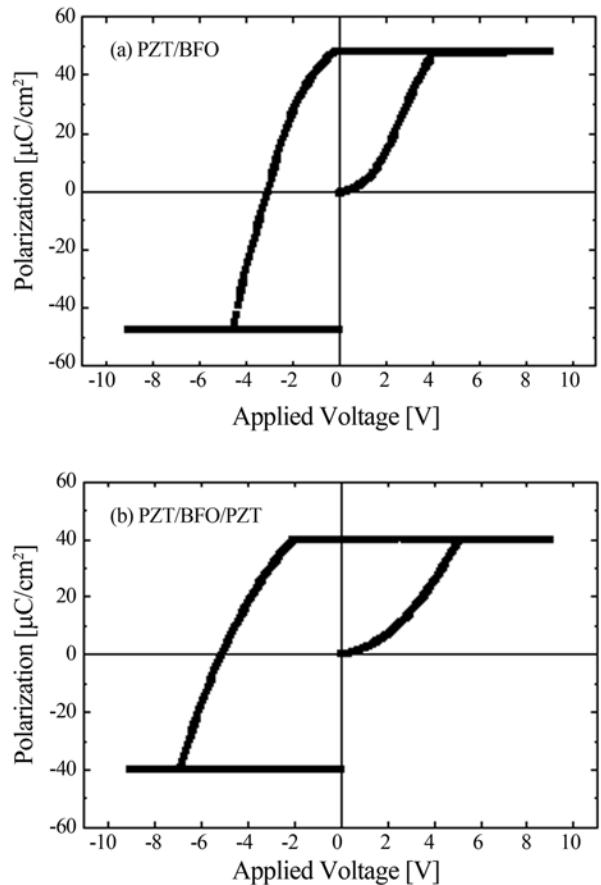


Fig. 4. Polarization-electric field hysteresis loops for (a) PZT/BFO film and (b) PZT/BFO/PZT film.

lower electrodes. PZT/BFO multilayer thin films exhibit a low remanent polarization and high coercive field compared with the PZT/BFO/PZT thin films. The remanent polarizations of PZT/BFO and PZT/BFO/PZT multilayer thin films are 47.85 mC/cm^2 and 39.97 mC/cm^2 , respectively. We consider that there is a coexistence of the PZT phase and BFO phase or the presence of nonstoichiometric PZT or BFO phases at the interfaces between PZT and BFO layers. Also Pb, Zr, Ti, Bi and Fe ions diffused into the adjacent PZT and BFO layers and Pb diffusion into the Pt bottom electrode was observed [10]. From these results, we inferred that the mixed phases or nonstoichiometric phases of the PZT and BFO compositions were formed at each interface of PZT and BFO films and a Pb-deficient interfacial layer was formed at the layer adjacent to the bottom electrode, respectively.

Conclusions

In this paper, PZT/BFO multilayer thin films were prepared by a sol-gel method by alternately using $\text{Pb}(\text{Zr}_{0.52}\text{Ti}_{0.48})\text{O}_3$ and BiFeO_3 alkoxide solutions. The thickness of BFO and PZT film by one-cycle of drying/sintering was approximately 40 nm and all films consist of fine grains with a relatively flat surface morphology. We think that the crystal growth of an upper layer can be influenced by the lower layers and the crystallization behavior of the resultant film has been controlled by choosing the initial layer or seeding layer. All the films showed hysteresis loops with high rectangularity. The remanent polarizations of PZT/BFO

and PZT/BFO/PZT multilayer thin films are 47.85 mC/cm^2 and 39.97 mC/cm^2 , respectively. We consider that there is a coexistence of the PZT phase and BFO phase or the presence of nonstoichiometric PZT or BFO phases at the interfaces between PZT and BFO layers.

Acknowledgement

This work was supported by the Korea Research Foundation (KRF) grant funded by the Korea government (MEST). (No. 2009-0077690)

References

1. G.A. Smolenskii and I. Chupis, Sov. Phys. Usp. 25 (1982) 475-493.
2. S.K. Singh, H. Ishiwara, K. Sato and K. Maruyama, J. Appl. Phys. 102 (2007) 094109-094113.
3. T. Kawae, Y. Terauchi, H. Tsuda, M. Kumeda and A. Morimoto, Appl. Phys. Lett. 94 (2009) 112904-1-3.
4. J.K. Kim, S.S. Kim, W.J. Kim, A.S. Bhalla and R. Guo, Appl. Phys. Lett. 88 (2006) 132901-1-3.
5. Y.W. Li, J.L. Sun, J. Chen, X.J. Meng and J.H. Chu, Appl. Phys. Lett. 87 (2005) 182902-1-3.
6. T. Ozaki and S. Mori, Jap. J. Appl. Phys. 48 (2009) 09KC07-1-4.
7. S.G. Lee and Y.H. Lee, Thin Solid Films 353 (1999) 244-248.
8. ICSD Coll. Code 90476.
9. Y. Matsuo and H. Sasaki, J. Am. Ceram. Soc. 48 (1965) 289-291
10. S.G. Lee, K.T. Kim and Y.H. Lee, Thin Solid Films 372 (2000) 45-49.